Revealing Dynamic Mechanisms of Cell Fate Decisions From Single-Cell Transcriptomic Data

Jiajun Zhang [1,2], Qing Nie [3,4] and Tianshou Zhou [1,2]*

[1] School of Mathematics, Sun Yat-Sen University, Guangzhou, China, [2] Guangdong Province Key Laboratory of Computational Science and School of Mathematics and Computational Science, Sun Yat-Sen University, Guangzhou, China, [3] Department of Developmental and Cell Biology, University of California, Irvine, Irvine, CA, United States, [4] Department of Mathematics, University of California, Irvine, Irvine, CA, United States

Cell fate decisions play a pivotal role in development, but technologies for dissecting them are limited. We developed a multifunction new method, Topographer, to construct a "quantitative" Waddington's landscape of single-cell transcriptomic data. This method is able to identify complex cell-state transition trajectories and to estimate complex cell-type dynamics characterized by fate and transition probabilities. It also infers both marker gene networks and their dynamic changes as well as dynamic characteristics of transcriptional bursting along the cell-state transition trajectories. Applying this method to single-cell RNA-seq data on the differentiation of primary human myoblasts, we not only identified three known cell types, but also estimated both their fate probabilities and transition probabilities among them. We found that the percent of genes expressed in a bursty manner is significantly higher at (or near) the branch point (~97%) than before or after branch (below 80%), and that both gene-gene and cell-cell correlation degrees are apparently lower near the branch point than away from the branching. Topographer allows revealing of cell fate mechanisms in a coherent way at three scales: cell lineage (macroscopic), gene network (mesoscopic), and gene expression (microscopic).

Keywords: cell fate decision, single-cell data, developmental landscape, cell-type dynamics, cellular process

INTRODUCTION

Multi-cell organisms start as a single cell that matures through complex dynamic processes involving multiple cell fate decision points, leading to functionally different cell types, many of which have yet to be defined (Trapnell, 2015). While cellular processes such as proliferation, differentiation, and reprogramming are governed by complex gene regulatory programs, each cell makes its own fate decisions by integrating a wide array of signals and executing a complex choreography of gene regulatory changes (Moris et al., 2016; Tanay and Regev, 2017). Since the structure of a multi-cell tissue is tightly linked with its function (Perié et al., 2015), elucidating the integrative (from gene to cell) mechanism of cell fate decisions is crucial yet challenging.

Single-cell measurement technologies (Svensson et al., 2017; Ziegenhain et al., 2017) which can simultaneously measure the expressions of many genes in a large number of single cells, provide an unprecedented opportunity to elucidate developmental pathways and dissect cell fate decisions.

Several algorithms [see a recent review (Saelens et al., 2019)] have been developed to organize single cells in pseudo-temporal order based on transcriptomic divergence and cell-state classification. It has been a major challenge to illuminate the dynamic mechanisms of cellular programs governing fate transitions from single-cell data that lacks temporal information (Trapnell, 2015). The current methods have mainly focused on identifying trajectories between the most phenotypically distant cell states, and they are usually less robust in reconstructing trajectories from early states towards intermediate or transitory cell states [e.g., Wishbone (Setty et al., 2016), Diffusion Pseudotime (Haghverdi et al., 2016), Cycler (Gut et al., 2015), and CellRouter (Lummertz da Rocha et al., 2018)]. Some of the methods have focused on gaining insights into the regulatory mechanisms driving cell differentiation [e.g., Monocle (Trapnell et al., 2014), ERA (Kafri et al., 2013), Waterfall (Shin et al., 2015), and PIDC (Chan et al., 2017)], and they seem not to consider how discontinuous, stochastic fate transition events are driven by the dynamic nature of the developmental landscape (which can change in response to activity of gene regulatory networks and extracellular signals) and reflected in the observed increased transcriptional heterogeneity at transition points. In all the existing methods, cell-type dynamics are mainly characterized qualitatively, providing little quantitative information on in-depth characterization of complex cellular ecosystems involving cell fate decisions. For a system of multiple cell fate decision points, it has been difficult for the current methods to estimate cell types and their transitions. How fate transitions in the single cell data are related to cell-state gene regulatory networks and the characteristics of transcriptional bursting remains largely unknown.

To overcome the above challenges and to address the important issues on cell fate decisions, we developed *Topographer*, an integrated pipeline. It first constructs a data-driven "quantitative" (i.e., each cell is endowed with spatiotemporal information) developmental landscape, which provides a global view for differentiation processes together with the cartoon landscapes (Waddington, 1957) and the model-driven landscapes (Wang et al., 2011; Li and Wang, 2013; Li and Wang, 2013; Li and Wang, 2014; Li and Wang, 2015), and then reveals stochastic dynamics of cell types by estimating both their fate probabilities and transition probabilities among them, and infers dynamic characteristics of transcriptional bursting kinetics along the identified developmental trajectory. In addition, it can also both identify various branched (e.g., bi- and tri-) cell-state transition trajectories with multiple branching points from single-cell data and infer networks of marker genes and their pseudo-temporal changes. Together, *Topographer* enables construction of complex cell lineages, resolving intermediate developmental stages, and revealing multilayer mechanisms of cell fate decisions in a coherent way at three different levels: cell lineage, gene network, and transcriptional burst (referring to **Supplementary Figure 1**).

We demonstrated effectiveness of *Topographer* by analyzing single-cell RNA-seq data on the differentiation of primary human myoblast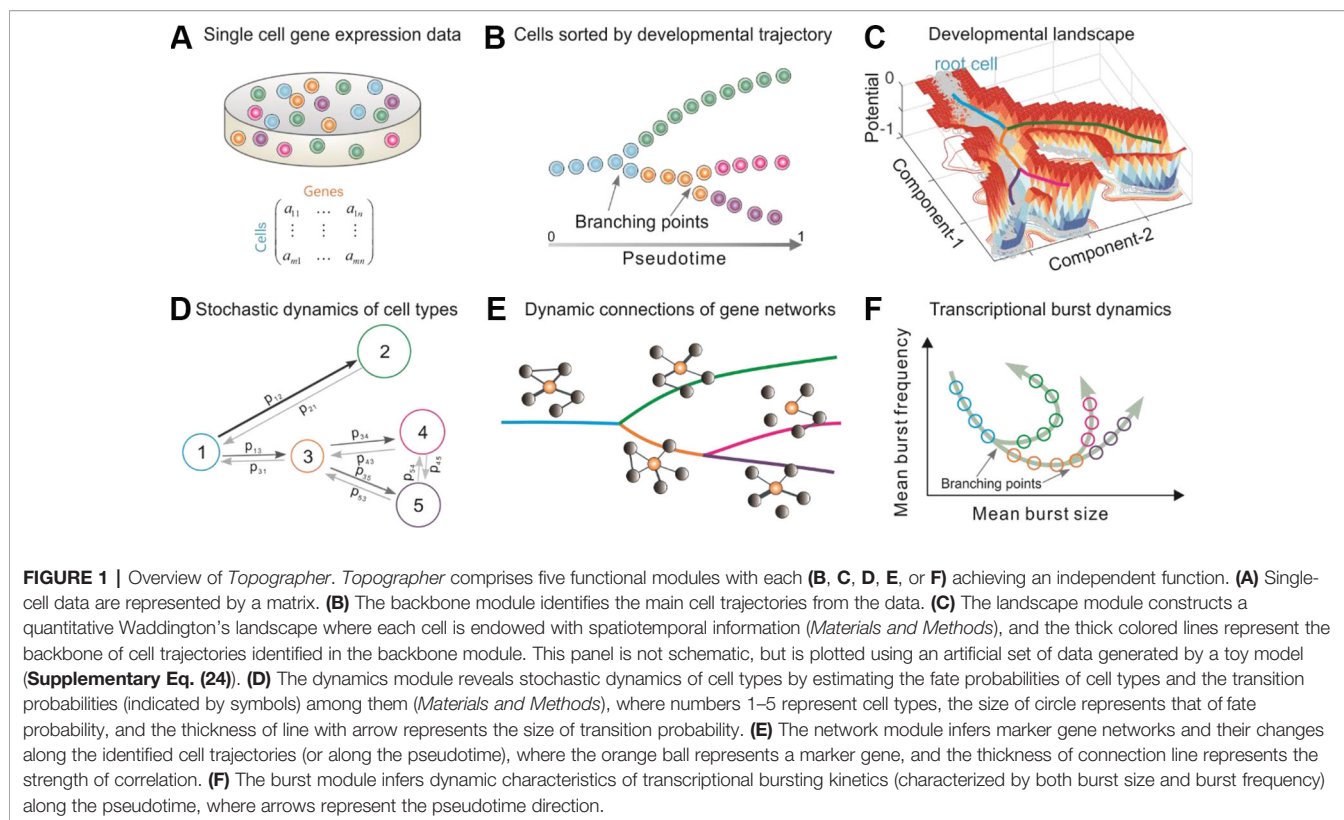s (Trapnell et al., 2014) while showing applications to other examples in **Supplementary Information**. We first identified three known cell types: proliferating cells, differentiating myoblasts, and interstitial mesenchymal cells, and then constructed a quantitative developmental landscape where each cell is endowed with spatiotemporal information. Furthermore, by estimating the fate probabilities of the identified cell types and transition probabilities among them, we found that the probability of transition from the proliferating cell type to the interstitial mesenchymal cell type was approximately twice that of transition from the former to the differentiating myoblast type, and that the fate probability of the differentiating myoblast type was approximately equal to that of the interstitial mesenchymal cell type. We also found that the relative number of the genes expressed in a bursty manner was apparently higher at (or near) the branch point (~97%) than before or after branch (below 80%). In addition, the mean burst size (MBS)/mean burst frequency (MBF) monotonically decreased/increased before branch but monotonically increased/decreased after branch, with the identified trajectories.

RESULTS

The Outline of Topographer

In order to infer the stochastic dynamics of cell fate decisions from single-cell transcriptomic data, *Topographer* makes the following assumption about the data: the information on the entire development process is adequate, or a snapshot of primary tissue represents a complete developmental process. The data need pre-processing (**Supplementary Information** for detail) so that *Topographer* achieve a good performance. The overall *Topographer*, a multifaceted single-cell analysis platform, comprises five functional modules: (Trapnell, 2015) the backbone module (**Figure 1B**); (Tanay and Regev, 2017) the landscape module (**Figure 1C**); (Moris et al., 2016) the dynamics module (**Figure 1D**); (Perié et al., 2015) the network module (**Figure 1E**); and (Svensson et al., 2017) the burst module (**Figure 1F**). The backbone module is independent of the remaining 4 modules that depends on the former since they make use of information on cell-state transition trajectories identified in the first module. All the five modules are logically related but each module achieves an independent function.

Two important notes on this method are (Trapnell, 2015) *Topographer* is unsupervised and needs no prior knowledge of specific genes that distinguish cell fates, and is thus suitable for studying a wide array of dynamic processes involving fate transitions. (Tanay and Regev, 2017) Except for the backbone module, the other four functional modules only use the pseudotime information derived in that module (*Materials and Methods*), so they can also use the result on pseudo-temporal ordering of single cells obtained by other existing algorithms (Saelens et al., 2019) to achieve their respective purposes. However, the backbone module is established based on a different approach (see the following content for details), and has its own advantages, e.g., it can identify not only cell-state

FIGURE 1 | Overview of *Topographer*. *Topographer* comprises five functional modules with each (**B**, **C**, **D**, **E**, or **F**) achieving an independent function. (**A**) Single-cell data are represented by a matrix. (**B**) The backbone module identifies the main cell trajectories from the data. (**C**) The landscape module constructs a quantitative Waddington's landscape where each cell is endowed with spatiotemporal information (*Materials and Methods*), and the thick colored lines represent the backbone of cell trajectories identified in the backbone module. This panel is not schematic, but is plotted using an artificial set of data generated by a toy model (**Supplementary Eq. (24)**). (**D**) The dynamics module reveals stochastic dynamics of cell types by estimating the fate probabilities of cell types and the transition probabilities (indicated by symbols) among them (*Materials and Methods*), where numbers 1–5 represent cell types, the size of circle represents that of fate probability, and the thickness of line with arrow represents the size of transition probability. (**E**) The network module infers marker gene networks and their changes along the identified cell trajectories (or along the pseudotime), where the orange ball represents a marker gene, and the thickness of connection line represents the strength of correlation. (**F**) The burst module infers dynamic characteristics of transcriptional bursting kinetics (characterized by both burst size and burst frequency) along the pseudotime, where arrows represent the pseudotime direction.

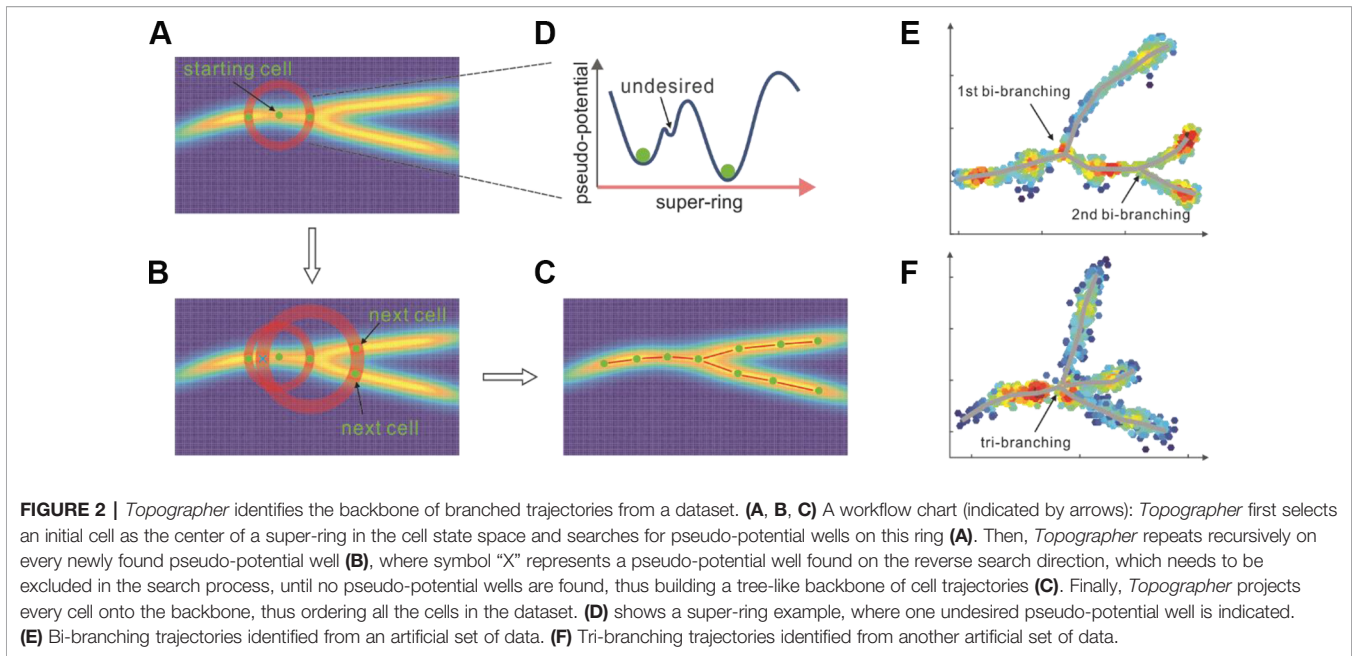transition trajectories with multiple branching points, but also intermediate or transitory cell states.

Below we introduce each of the five functional modules separately (*Materials and Methods* give more details and **Supplementary Information** provides a complete description).

Identifying the Backbone of Cell Trajectories From Single-Cell Data

The backbone module is a fast and local pseudo-potential-based algorithm. Here the pseudo-potential is defined as the negative of the logarithm of a local density function (Eq. (1), *Materials and Methods*), which aims to identify the "backbone" (i.e., "planimetric" contour) of cell-state transition trajectories cross development and find valley floors in a developmental landscape from single-cell data.

Starting from an initial cell (**Figure 2A**) selected either based on the global minimal pseudo-potential or the prior knowledge, *Topographer* calculates an adaptive step (**Supplementary Eq. (5)**) and searches for pseudo-potential wells (i.e., "pits" where pseudo-potentials are relatively lower) on a super-ring (i.e., a high-dimensional circular tube, referring to **Figure 2A**, which shows a flatten super-ring) centered at this initial cell and with the radius equal to the step length (also **Figure 2A**). In this search method, which clusters cells on super-rings, cluster centers are characterized by a lower pseudo-potential than their neighbors and by a relatively larger distance from points with lower pseudo-potentials (e.g., the only two pseudo-potential wells with "green ball" in **Figure 2D** are desired),

providing the basis of a procedure to find pseudo-potential wells on a super-ring. In this procedure, the number of pseudo-potential wells arises naturally, outliers are automatically spotted, and pseudo-potential wells are recognized regardless of their shape and the dimensionality of the space in which they are embedded. We stress that although there is an analogy between our method and a density-based approach developed originally by Rodriguez and colleagues (Rodriguez and Laio, 2014), the difference is that the former is carried out on a super-ring rather than in the full cell state space. Clearly, if the number of the found pseudo-potential wells (but not including the one found on the "reverse" search direction) is more than one, this implies the occurrence of branch. The segments linking the center and the newly found pseudo-potential well/or wells on the super-ring can be viewed as part/or parts of the entire developmental trajectory. Similar processes are repeated recursively on sequential super-rings along search directions until no new pseudo-potential wells are found (**Figure 2B**). By linking all the centers and all the pseudo-potential wells found on super-rings, *Topographer* thus, builds a tree-like developmental backbone (**Figure 2C**). Note that the identified backbone is actually a projection of the pseudo-potential landscape. By projecting every cell onto this backbone (see subsection *Cell Projection and Pseudotime Assignment, Materials and Methods*) and by selecting a root node in the tree (e.g., based on the prior knowledge), *Topographer* thus orders all the single cells in the dataset, and equips each cell with a pseudotime if this root node is set as an

FIGURE 2 | *Topographer* identifies the backbone of branched trajectories from a dataset. **(A, B, C)** A workflow chart (indicated by arrows): *Topographer* first selects an initial cell as the center of a super-ring in the cell state space and searches for pseudo-potential wells on this ring **(A)**. Then, *Topographer* repeats recursively on every newly found pseudo-potential well **(B)**, where symbol "X" represents a pseudo-potential well found on the reverse search direction, which needs to be excluded in the search process, until no pseudo-potential wells are found, thus building a tree-like backbone of cell trajectories **(C)**. Finally, *Topographer* projects every cell onto the backbone, thus ordering all the cells in the dataset. **(D)** shows a super-ring example, where one undesired pseudo-potential well is indicated. **(E)** Bi-branching trajectories identified from an artificial set of data. **(F)** Tri-branching trajectories identified from another artificial set of data.

initial moment (without loss of generality, the full pseudotime may be set as the interval between 0 and 1).

Figures 2E, **F** showed respectively a doubly bi-branched trajectory identified from one simulated dataset and a tri-branched trajectory identified from another artificial set of data. **Figure 3A** below demonstrated a two-dimensional projection of the *de novo* cell trajectories identified from single-cell RNA-seq data on the differentiation of primary human myoblasts and **Figure 3B** demonstrated the evolutions of five marker genes (MYOG, MYF5, MYH2, CDK1, and MEF2C) with branches along the along the pseudotime. **Supplementary Figure 12** and **Figure 14** demonstrated results of other two examples, which further showed the power of *Topographer* in pseudo-temporally ordering single cells in single-cell data.

Because of its ability to find pseudo-potential wells on super-rings, *Topographer* can identify *de novo* developmental trajectories with non-, bi-, and multi-branches (referring to **Figures 1E**, **F**) (note: a low resolution of experimentally sampling data may lead to tri-branches).
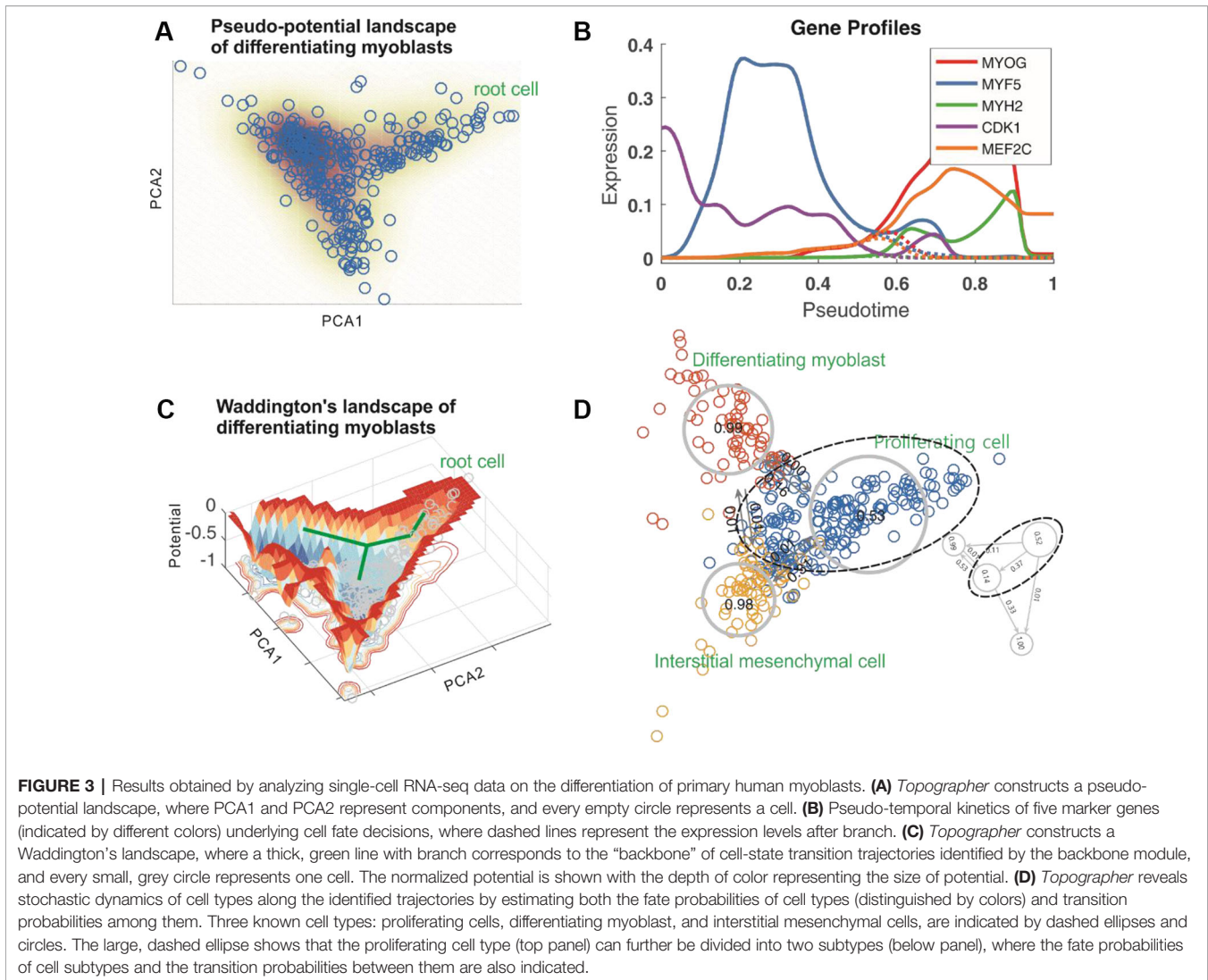
Constructing a Quantitative Developmental Landscape of Single-Cell Data

The backbone module used pseudo-potentials to construct the contour of cell-state transition trajectories, which extracted the information on both branch and cellular ordering from single-cell data. Note that this kind of potential would not correctly reflect transitions between cells since the probability fluxes would exist between them due to cell division, cell death and/or other factors, and have been quantified from gene network models (Li and Wang, 2014). For example, precursor cells should in principle have higher pseudo-potentials (Eq. (8), *Materials and Methods*) in a developmental landscape in contrast to their

generations, but if the precursor cells have higher densities, they have lower pseudo-potentials. Apparently, both are inconsistent. In addition, pseudo-potential lacks the temporal information on differentiation or development.

Because of both the above shortcoming of pseudo-potential and the intuition of the Waddington's developmental landscape (in fact, it has been extensively viewed as a powerful metaphor for how differentiated cell types emerge from a single, totipotent cell 1), the landscape module (an algorithm) is designed to construct a "stereometric" developmental landscape (by "stereometric" we mean that each cell is loaded with spatiotemporal information) in contrast to the "planimetric" contour identified by the backbone module. This constructed landscape can provide a more intuitive understanding for the whole developmental process. The principle of the landscape module is simply stated below.

Since single-cell data are noisy due to both cellular heterogeneity and gene expression noise, transitions among the cells scattered randomly in the cell state space can be considered as a random walker (this consideration is inspired by Rosvall and Bergstrom's work 23). *Topographer* first constructs a weighted directed graph based on the pseudotime information obtained in the backbone module, and then defines a conditional probability (Eq. (Svensson et al., 2017), *Materials and Methods*) that the random walker moves from one cell to another with relative weight strengths. Then, *Topographer* estimates the visit probability for each cell by solving a master equation (Eq. (6), *Materials and Methods*), and determines the potential of every cell in the dataset, where the potential is defined as the negative of the logarithm of the visit probability, seeing Eq. (8) with Eq. (7) in *Materials and Methods*. All these potentials are then used to construct a Waddington's developmental landscape. For this, a dimension reduction (van der Maaten and Hinton, 2008) is used for visualization, the nearest neighbor interpolation is used to fit a landscape function of

FIGURE 3 | Results obtained by analyzing single-cell RNA-seq data on the differentiation of primary human myoblasts. **(A)** *Topographer* constructs a pseudo-potential landscape, where PCA1 and PCA2 represent components, and every empty circle represents a cell. **(B)** Pseudo-temporal kinetics of five marker genes (indicated by different colors) underlying cell fate decisions, where dashed lines represent the expression levels after branch. **(C)** *Topographer* constructs a Waddington's landscape, where a thick, green line with branch corresponds to the "backbone" of cell-state transition trajectories identified by the backbone module, and every small, grey circle represents one cell. The normalized potential is shown with the depth of color representing the size of potential. **(D)** *Topographer* reveals stochastic dynamics of cell types along the identified trajectories by estimating both the fate probabilities of cell types (distinguished by colors) and transition probabilities among them. Three known cell types: proliferating cells, differentiating myoblast, and interstitial mesenchymal cells, are indicated by dashed ellipses and circles. The large, dashed ellipse shows that the proliferating cell type (top panel) can further be divided into two subtypes (below panel), where the fate probabilities of cell subtypes and the transition probabilities between them are also indicated.

two variables in a 2-dimension space, and a Gaussian kernel is applied to smooth interpolation (see subsection *Scatter Plot of Developmental Landscape, Materials and Methods* or subsection *Scatter Plot of Developmental Landscape*, **Supplementary Information**). In this constructed landscape, each cell is equipped with both potential and pseudotime: two important attributes of a cell. Therefore, the identified backbone of cell-state transition trajectories, which considers pseudo-potentials rather than potentials, can be viewed as an aerial photograph of the constructed Waddington's developmental landscape (comparing **Figure 3A** with **Figure 3C**).

To demonstrate effectiveness of the landscape module, we analyzed two examples: the one for the same set of artificial data used in **Figure 2E**, with the result demonstrated in **Figure 1C**, and the other for a set of single-cell data on the differentiation of primary human myoblasts, with the results demonstrated in **Figure 3C**. Consequently, we constructed a Waddington's developmental landscape shown in **Figure 3C** from a realistic set of data. Note

that it is different from a cartoon landscape, such as **Figure 5** in references (Olsson et al., 2016). **Supplementary Figure 13** demonstrated another Waddington's developmental landscape constructed using single-cell data on the development of somatic stem cells.

It is worth noting that: (1) In contrast to the backbone module that is mainly used to identify a main "road" but ignores "bumpiness" of the road, the landscape module considers both the road (actually a valley floor of the constructed Waddington's landscape) and its bumpiness (reflected by the height of potentials). (2) Both modules can identify cell-state transition trajectories from a dataset, but the former uses pseudo-potentials that rely on neither pseudotime nor cell type whereas the latter uses potentials that depend on both pseudotime and cell type (Eq. (8) with Eq. (4), *Materials and Methods*). (3) Pseudo-potential cannot correctly reflect the motion of a "ball" (i.e., progenitor cell progression) in the constructed Waddington's landscape in which the ball has lower potential at the beginning than at the end, since a lower cell density

means a higher pseudo-potential. **Supplementary Figure 5** shows a difference between potential and pseudo-potential.

Estimating Fate and Transition Probabilities From Single-Cell Data

Gene regulatory programs underlying cell fate decisions drive one cell type toward another. Quantifying such a transition using single-cell data is challenging due to both cellular heterogeneity and the noise in gene expression in the data.

In order to estimate cell-type dynamics characterized by fate and transition probabilities from single-cell RNA-seq data, it is first needed to determine types of the cells in the dataset. *Topographer* determines cell type according to the following rules: (1) each branch of the identified developmental trajectory is viewed as a cell type with a different branch representing a different cell type; (2) At each branch, the found potential well is taken as a cell subtype with a different potential well representing a different cell subtype. Thus, the number of cell types is equal to the number of branches whereas the total number of cell subtypes is equal to that of potential wells. We will not distinguish cell type and cell subtype unless confusion arises. The cell types determined using this method depend on the shapes of rugged potential wells (prior knowledge can provide additional information in some cases). Therefore, the classification of cell types in this approach is relative rather than "absolute". For example, in **Figure 3D**, the proliferating cell type indicated by a dashed ellipse can be further divided into two subtypes. In some situations, a potential well in the constructed Waddington's developmental landscape might not be apparent, but still represents a small cell subtype or an intermediate cell state, which may have important biological implications.

In the dynamics module, *Topographer* considers that transitions among the cells scattered randomly in the cell state space is a random walker who randomly moves from a cell state to another, and then estimates two kinds of probabilities: the fate probability for each cell type and the transition probabilities between every two cell types (*Materials and Methods*). In these estimations, *Topographer* makes use of the cell-state transition trajectories identified in the backbone module.

Specifically, *Topographer* first defines a weight of the directed edge from one cell to another based on the pseudotime (Eq. (4), *Materials and Methods*), and then uses all the possible weights to estimate the visit probability that the random walker visits a cell in the state space, and further the conditional probability defined as a relative link weight (Eq. (5), *Materials and Methods*). With these two kinds of probabilities, *Topographer* further estimates the probability that the random walker visits each cell type, and the transition probabilities between every two cell types (Eq. (9), *Materials and Methods*). These estimations indicate that transitions between cell types are in general not deterministic, but stochastic (referring to **Figure 3D**). In addition, *Topographer* estimates the fate probability of each cell type (Eq. (12), *Materials and Methods*).

In order to demonstrate stochastic cell-type dynamics estimated by the dynamics module, we again analyzed a simulated data with results shown in **Supplementary Figure 6**, and a realistic set of single-cell RNA-seq data on the differentiation of primary human myoblasts with results demonstrated in **Figure 3D** (as well as another realistic set of single-cell RNA-seq data on the development of somatic stem cells, with results demonstrated in **Supplementary Figure 13**). From **Figure 3D**, we observed that the fate probability (~0.53) for the proliferating cell type is about the half of that for the differentiating or interstitial mesenchymal cell type (this is not strange since the proliferating cells are root ones), but the fate probabilities for the latter two (~0.99 and ~0.98, respectively) are approximately equal. In addition, the proliferating cells differentiate into the differentiating cells at the ~0.16 probability, but the inverse differentiation probability is very small (~0.001). On the other hand, the proliferating cells differentiate into the interstitial mesenchymal cells at the ~0.31 probability but the inverse differentiation probability is also very small (~0.01), implying that the proliferating cells tend to differentiate into the interstitial mesenchymal cells. **Figure 3D** also showed the fate probabilities of cell subtypes and the transition probabilities between them (low panel).
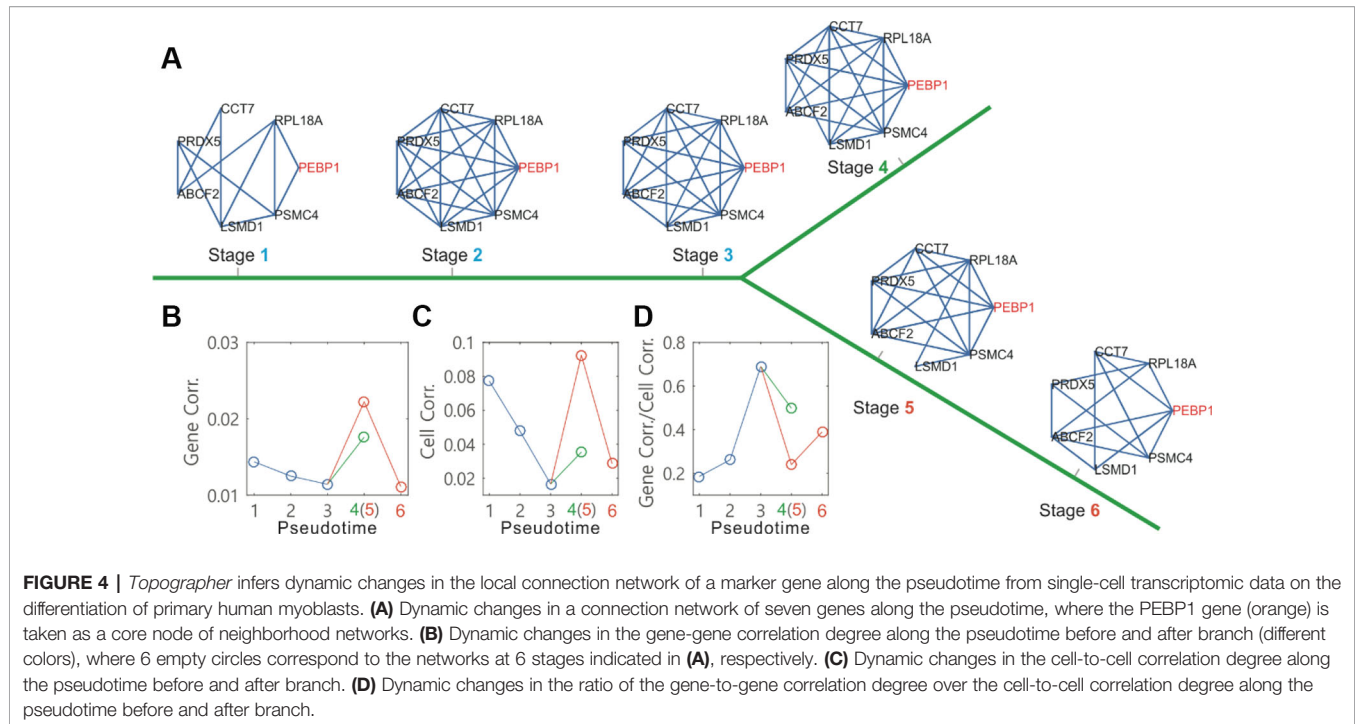
Apart from the above three main functional modules, *Topographer* can also infer both marker gene networks and their pseudo-temporal changes as well as pseudo-temporal characteristics of transcriptional bursting kinetics. We point out that these inferences can in turn be used to infer whether and when (along pseudotime) the branches of a developmental trajectory occur.

Inferring Marker Gene Networks and Their Pseudo-Temporal Changes

The network module aims to infer the trend of how marker gene networks dynamically change along the identified cell-state transition trajectories. For this, *Topographer* uses the network neighborhood analysis method (Li and Horvath, 2007) (or section *The Network Module Infers Marker Gene Networks and Their Pseudo-Temporal Changes, Materials and Methods*) to explore dynamic changes in gene regulatory networks (GRNs) across development.

First, *Topographer* uses GENIE3 (Huynh-Thu et al., 2010) to generate a series of GRNs along the pseudotime. Then, based on these GRNs, *Topographer* further analyzes the covariation partners of some particular gene (or genes) using a topological network analysis scheme (Klein et al., 2015) that can identify those genes most closely correlated with a given gene (or genes) of interest and most closely correlate to each other (See *Materials and Methods* for details). We stress that before these two steps, transcriptomic data of interest need pre-processing (**Supplementary Information**) since they are noisy and would contain many zeros that must be removed in our method.

Here, we used the network module to analyze single-cell data on the differentiation of primary human myoblasts, and obtained dynamic changes in the connections of marker gene networks along the identified cell-state transition trajectories (**Figure 4A**, where the PEBP1 gene is a core node of the networks). From the dependences of mean gene-gene correlation degrees (**Figure 4B**) and mean cell-cell correlation degrees (**Figure 4C**) on the pseudotime, we observed that before branch, both degrees were

FIGURE 4 | *Topographer* infers dynamic changes in the local connection network of a marker gene along the pseudotime from single-cell transcriptomic data on the differentiation of primary human myoblasts. **(A)** Dynamic changes in a connection network of seven genes along the pseudotime, where the PEBP1 gene (orange) is taken as a core node of neighborhood networks. **(B)** Dynamic changes in the gene-gene correlation degree along the pseudotime before and after branch (different colors), where 6 empty circles correspond to the networks at 6 stages indicated in **(A)**, respectively. **(C)** Dynamic changes in the cell-to-cell correlation degree along the pseudotime before and after branch. **(D)** Dynamic changes in the ratio of the gene-to-gene correlation degree over the cell-to-cell correlation degree along the pseudotime before and after branch.

a monotonically decreasing function in pseudotime (the blue line, **Figure 4B** or **C**), but after branch, each became first monotonically increasing and then monotonically decreasing on one branch (the orange line, **Figure 4B** or **C**), and monotonically increasing on the other branch (the green line, **Figure 4B** or **C**). However, the change tendency for the ratio of the gene-gene correlation degree over the cell-cell correlation degree was just opposite to that described above (**Figure 4D**). Note that a decrease in the overall gene-gene correlation indicates that there are less regulations in the cells. And a decrease in the cell-cell correlation reflects an increase in the amplitude of random fluctuation in gene expression due to the weakening attracting force in the flattening basin of attraction prior to the bifurcation. The ratio of GeneCorr/CellCorr is a quantitative index for predicting critical transitions. This index increases toward a maximum when cells go through the critical state transition that is similar to the index proposed by Chen et al., (2012) and Mojtahedi et al., (2016).

Inferring Pseudo-Temporal Characteristics of Transcriptional Bursting Kinetics

Transcription occurs often in a bursty manner, and single-cell measurements have provided evidence for transcriptional bursting both in bacteria and in eukaryotic cells (Larson, 2011). By analyzing a simplified stochastic model of gene expression, Xie, et al. previously showed (Friedman et al., 2006) that the number of mRNAs produced in the bursty fashion following a Gamma distribution determined by two parameters: MBF (i.e., the mean number of mRNA production bursts per cell cycle) and MBS (i.e., the average size of the mRNA bursts). We point out that if a Beta-Poisson distribution (Kim and Marioni, 2013) is used or other distributions are used, the result is similar (data are not shown).

There is great interest in analyzing single cell data to understand the transcriptional changes that occur as cells differentiate and the genes and regulatory mechanisms controlling differentiation processes and cell-fate transition points (Moignard and Göttgens, 2016; Tanay and Regev, 2017). The burst module is designed to infer the trend of how transcriptional bursting kinetics dynamically changes across development. For this, *Topographer* uses the maximum likelihood method (Cam, 1991) to infer the two parameters of MBF and MBS from single-cell RNA-seq data (see section *The Burst Module Infers Pseudo-Temporal Characteristics of Transcriptional Bursting Kinetics, Materials and Methods*), thus revealing dynamic characteristics of transcriptional bursting kinetics before branch, near the branching point and after branch of the developmental trajectory.

We used the burst module to analyze single-cell data on the differentiation of primary human myoblasts. **Figures 5A–E** showed how the cells at four pseudotime points (two before branch, one at branch point, and one after branch) were distributed in the logarithmic plane of BF and BS. A reference system (two orthogonal blue lines indicated by blue: the horizontal line for BF and the vertical line for BS) was used to guide visual comparison between the rates (i.e., the percents indicated) of gene numbers over the total gene number at a particular pseudotime point. The four quadrants of the reference system clearly showed how the genes in the dataset were expressed, e.g., the fourth quadrant showed that the genes were expressed in a manner of high frequency (i.e., the BF is more than 0.33) and small burst (i.e., the BS number is less than 200). We observed that the genes expressed in a bursty manner (i.e.,
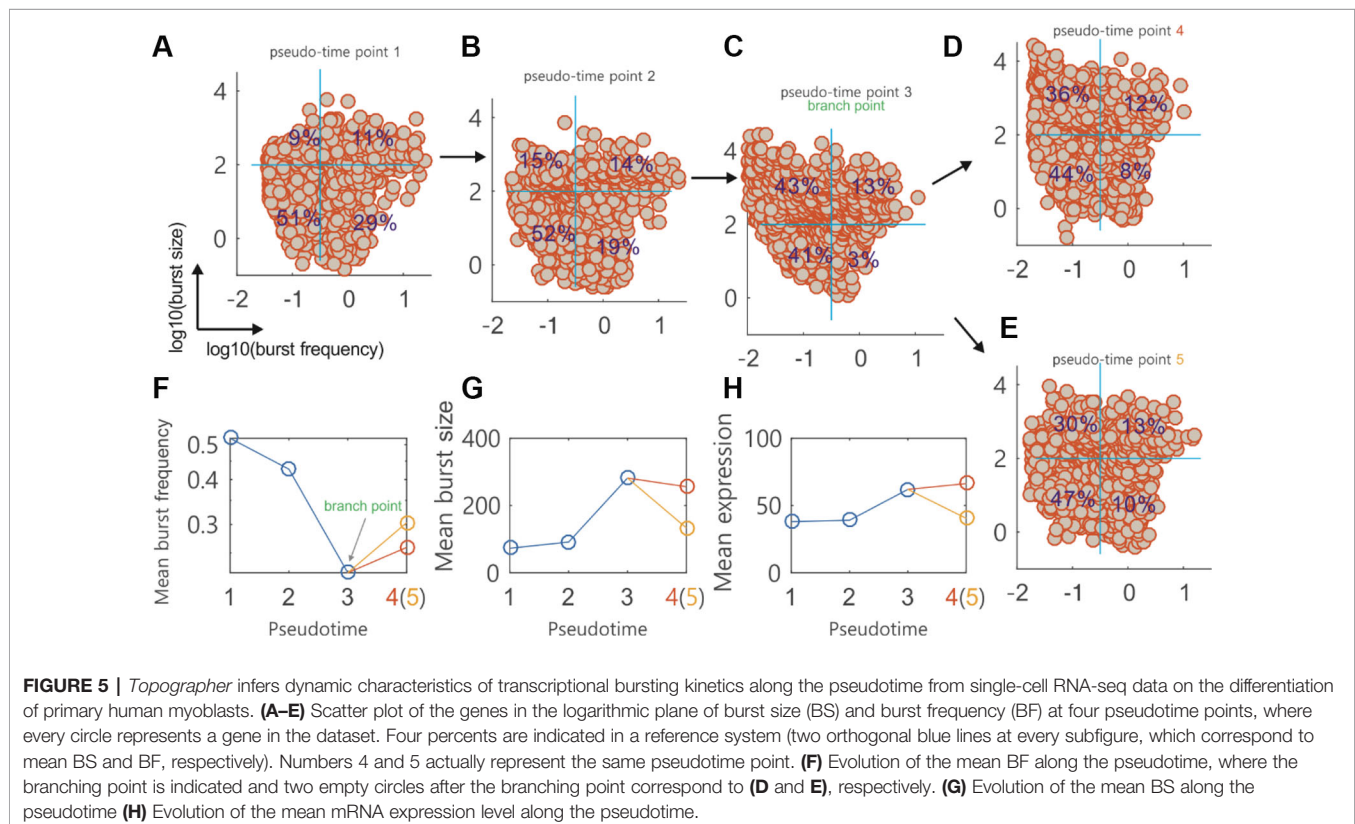
the other three cases except for the case in the fourth quadrant) were more at the branching point (97%) than before or after branch (approximate or below 80%). In other words, the percent of the genes expressed with high frequency and small burst was apparently lower at the branching point. From these figures, we can conclude that during the differentiation of primary human myoblasts, there are more genes expressed in a bursty manner at the branching point than before or after branch.

From the dependences of MBF and MBS on the pseudotime (**Figures 5F**, **G**), we observed that there were apparently different change trends before and after branch. **Figure 5H** showed the dependence of the mean mRNA expression level on the pseudotime, demonstrating a change tendency opposite to that of MBF. Although fundamentally similar to the change trend of MBS on the whole, the mean mRNA level (which is approximately equal to the product of the MBS and the MBF) for the branched pseudo trajectory of points 1, 2, 3, and 4 has an increasing tendency with the increase of the pseudotime (**Figure 5H**). These three subfigures implied that MBF or MBS can be taken as a better indicator of the branch occurrence than the mean mRNA expression level. They also imply that cell fate decisions would not be inferred from the changes in the mean gene expression levels but can be inferred from the changes in the transcriptional bursting kinetics characterized by BS and BF. Recently, Larsson, et al., showed that a separation of expression into bursting kinetics was required to identify the effects of core promoter elements on transcriptional dynamics that were masked at mean expression levels (Larsson, 2019).

DISCUSSION

We have developed a computational pipeline— *Topographer* for construction of developmental landscapes, identification of *de novo* continuous developmental trajectories, and quantification of fate transitions. One unique feature of *Topographer* is its capability of characterizing both transcriptional bursting kinetics and changes in connections of marker gene networks along developmental trajectory. When identifying the backbone of cell-state transition trajectories from single-cell data, *Topographer* was robust to the noise in the dataset (**Supplementary Figures 8–10**). When applied to the differentiation of primary human myoblasts, *Topographer* first constructed an intuitive developmental landscape for an order and timing of events that closely recapitulated previous studies of this system. In addition, it estimated the fate probabilities for cell types and the transition probabilities between them. Together, the results suggested that the fate transition during the differentiation of primary human myoblasts occurred in a probabilistic rather than deterministic manner, and the transitions between cell types might be unidirectional and bidirectional. These two new insights challenge the traditional view that the development of primary human myoblasts was tree-like or that the process from a predecessor to its generations was both deterministic and unidirectional (Svensson et al., 2017).

When ordering single cells, *Topographer* (like existing methods in the literature) needs to assume sufficient number of cells in the dataset because the backbone module is established essentially

FIGURE 5 | *Topographer* infers dynamic characteristics of transcriptional bursting kinetics along the pseudotime from single-cell RNA-seq data on the differentiation of primary human myoblasts. **(A–E)** Scatter plot of the genes in the logarithmic plane of burst size (BS) and burst frequency (BF) at four pseudotime points, where every circle represents a gene in the dataset. Four percents are indicated in a reference system (two orthogonal blue lines at every subfigure, which correspond to mean BS and BF, respectively). Numbers 4 and 5 actually represent the same pseudotime point. **(F)** Evolution of the mean BF along the pseudotime, where the branching point is indicated and two empty circles after the branching point correspond to **(D** and **E)**, respectively. **(G)** Evolution of the mean BS along the pseudotime **(H)** Evolution of the mean mRNA expression level along the pseudotime.

based on the estimation of cell density. A small number of cells (e.g., less than 100), would lead to inaccuracy of finding pseudo-potential well/or wells on a super-ring in the backbone module. As more cells can simultaneously be measured (Klein et al., 2015), the accuracy of *Topographer* will improve. In principle, *Topographer* can also be used to analyze other single-cell data such as mass cytometry data and single-cell PCR data (Bendall et al., 2011).

Cell fate decisions may involve hierarchy of cell types including intermediate cell states or cell subtypes. Identifying such (e.g. rare) sub-cell types is important yet challenging. *Topographer* has shown its ability to identify cell subtypes, which may correspond to shallow or small potential wells in the constructed developmental landscape (right below, **Figure 3D**). Moreover, *Topographer* can estimate the fate probability of each identified cell subtype and the transition probabilities between every two identified cell subtypes (right below, **Figure 3D**), which is one main advantage of *Topographer* compared to many existing methods (Saelens et al., 2019). In particular, *Topographer* enables identification of non-, bi-, and multi-branches (**Figures 2C, D**).

It is worth noting that *Topographer* only provides a general framework connecting three interplayed major components based on single-cell data: cell lineage committing dynamics (macroscopic), gene network dynamics (mesoscopic), and transcriptional bursting kinetics (microscopic). First, *Topographer* provides useful information on their relationships that are implied by the pseudotime, but this kind of time only reflects the impact of the former on each of the latter two. The issues of how and in what degree the inferred gene connection networks or/and transcriptional bursting kinetics influence or/and determine cell fates in the underlying developmental process, remain unexplored. In order to study the relationship between the mesoscope/microscope and the macroscope, a possible way is to establish the so-called balance equation (Wu and Tzanakakis, 2012). Second, in order to estimate the fate probabilities of cell types and the transition probabilities between them (Eq. (12) and Eq. (9), *Materials and Methods*, respectively), *Topographer* makes an assumption that the transition from one cell to another along a cell-state transition trajectory is linear (Eq. (4) in *Materials and Methods* or **Supplementary Eq. (6)**). In many cases, such transition may be nonlinear due to, e.g., cell-cell communication through signal molecules. Third, the traditional Waddington's landscape (e.g., tumor pathobiology 39) is often used as an intuitive tool to describe a differentiation process through the trajectory of a ball into branching valleys with each representing a developmental state (Furusawa and Kaneko, 2012). *Topographer* uses the potential of each cell to quantify developmental landscape, which allows estimation of the transition probabilities between cell types and their fate probabilities to characterize cell lineage committing dynamics. These probabilities have physical meanings as they actually represent the Krammer escape rates (van Kampen, 1992) between potential wells. However, how cell fate decisions including cell-state dynamics are related to Krammer escape rates remain unclear. Fourth, based on the transition probabilities between cell types, one can establish a model of cell population dynamics [referring to **Supplementary Eq. (21)**], and further study

stochastic state transitions from a dynamical-system perspective. Fifth, *Topographer* uses a simple Gamma distribution to infer transcriptional bursting kinetics. For this reference, a more reasonable distribution used would be a Beta-Poisson distribution, but the result is similar (data are not shown). In fact, our reference method is suitable to any distribution.

Finally, using "relatively smaller pseudo-potential and relatively larger distance" (*Materials and Methods*) as a rule in the backbone module is a robust approach in finding cell trajectories (referring to **Supplementary Figures 8–10**); In our method, the transitions among cells are considered as a random walker who moves randomly between the data points scattered in the cell state space. These two ground rules used in *Topographer* can be viewed as new principles of mining single-cell data to uncover mechanisms of cell fate decisions.

CONCLUSION

As the single-cell field progresses towards analyzing the transcriptomic data of large-scale individual cells in parallel, it will become increasingly important to develop statistical methods to reveal cell fate mechanisms in a coherent way at three levels: cell lineage (macroscopic), gene network (mesoscopic), and gene expression (microscopic). In this context, we anticipate that the *Topographer* presented here, and other related approaches, will be vital in maximizing the amount of biological insight that can be obtained from these data.

MATERIALS AND METHODS

The overall *Topographer*, a multifunctional algorithm, comprises five functional modules: the backbone module, the landscape module, the dynamics module, the network module, and the burst module. Main details of these modules are separately stated below and the complete description including data pre-processing is given in **Supplementary Information**.

The Backbone Module Identifies the Backbone of Cell-State Transition Trajectories From Single-Cell Data

Assume that there are m cells and n genes in single-cell RNA-seq data of interest, which can in principle be represented as m points in the n-dimensional space (X) of gene expression (called the cell state space for convenience).

The backbone module aims to identify the backbone of cell-state transition trajectories across development from the dataset. The essence is to find valley floors in a developmental landscape. Specifically, *Topographer* finds valleys with local minimal pseudo-potentials, where pseudo-potential is defined as

$$\tilde{E}(\boldsymbol{x}) = -\log \rho(\boldsymbol{x}) \tag{1}$$

with

$$\rho(\boldsymbol{x}) = \sum_{y \in X} \exp\left(-\frac{d(\boldsymbol{x}, \boldsymbol{y})^2}{2\sigma^2}\right). \tag{2}$$

In Eq. (2), d is the Euclidean distance between two state points x and y in the cell state space X (note: other kinds of distances are also suitable for *Topographer*). Note that ρ represents the local cell density, mostly accounting for the number of cells in a neighborhood defined by σ. The value of parameter σ is set as the corresponding quantile for all pair-wise distances of cell states in the dataset.

Roughly speaking, *Topographer* starts by cell state x_0 (i.e., an initial cell) and then searches for pseudo-potentials wells on super-rings (which are actually circular tubes in the cell state space) by recursively applying an extended version of the cluster algorithm (Rodriguez and Laio, 2014) Finally, all the centers of the super-rings are represented in a tree, T. Main details are stated below and more details are given in **Supplementary Information**.

Constructing a Developmental Tree

Starting by an initial cell that has the global minimal pseudo-potential or by the cell that the user chooses according to the prior knowledge, *Topographer* calculates an adaptive radius or an adaptive step length (see subsection *Setting Step Length*, **Supplementary Information**) and searches for pseudo-potential wells on a super-ring centered at this cell and with the radius (referring to **Figure 2A**). The search method (called the pseudo-potential well search algorithm) is based on the idea that cluster centers on the super-ring are characterized by a lower pseudo-potential than their neighbors and by a relatively larger distance from points with locally lower pseudo-potentials. Specifically, *Topographer* first defines

$$\delta(x) = \begin{cases} \max\limits_{y \neq x} d(x, y) & \text{if } \tilde{E}(x) = \min\limits_{y \in X} \tilde{E}(y) \\ \min\limits_{y : \tilde{E}(y) < \tilde{E}(x)} d(x, y) & \text{otherwise,} \end{cases} \qquad (3)$$

and then finds local pseudo-potential well/or wells on the super-ring, based on the combination of relatively smaller $\tilde{E}$ and relatively larger δ. Therefore, there is an analogy between the pseudo-potential well search algorithm and a density-based approach developed originally by Rodriguez and colleagues (Rodriguez and Laio, 2014). The segments linking the center and the pseudo-potential wells found on the super-ring can be taken as approximate part/or parts of the entire developmental trajectory.

Then, taking every found pseudo-potential well as the center of a new super-ring with a new adaptive radius, *Topographer* performs similar calculations as at the previous step, thus finding pseudo-potential well/or wells on this new super-ring. Again, the segments linking the new center and the newly found pseudo-potential wells on the new super-ring can be taken as other approximate part/or parts of the entire developmental trajectory. This process is repeated until no new pseudo-potential wells are found. By linking the cluster centers, *Topographer* thus builds a tree-like developmental backbone, which is actually composed of valleys.

Note that for a super-ring center, rather than the starting point, the newly found valleys would include valleys on the "reverse direction" in the processes of searching for local pseudo-potential wells on super-rings, which are not expected in our algorithm. To handle such an exception, *Topographer* excludes those valleys that are too close to the found valleys. In addition, any two newly found valleys with the distance of smaller than the step length are merged by discarding the valleys with larger pseudo-potentials. Such a

treatment may greatly improve the algorithm's robustness against the noise in the dataset (referring to **Supplementary Figures 8–10**).

Also note that a complete valley floor is constructed by terminating the recursive process for some super-ring on which no desired pseudo-potential wells can be found. Since no loops are assumed to exist in the developmental trajectory, there is definitely a boundary, implying that the search process necessarily stops within finite steps.

After the above search process is completed, all the found pseudo-potential valley floors are represented in an undirected acyclic graph (a tree with branches). To achieve better accuracy and coverage, *Topographer* refines a pseudo-potential valley tree by searching for pseudo-potential well/or wells on the line linking two centers on every edge of the tree (referring to **Supplementary Figures 9** and **10**). To that end, *Topographer* finishes construction of the backbone of a developmental tree from a given set of single-cell data.

Cell Projection and Pseudotime Assignment

After constructing a developmental tree, *Topographer* then projects every cell point in the cell state space onto some edge of the tree according to the shortest distance principle (i.e., the perpendicular distance from the cell point to the edge is shortest). Thus, every cell has its unique relative position in the identified backbone (or in the constructed tree).

Next, *Topographer* assigns a pseudotime for every cell in the dataset. Before that, however, it is needed to determine a root node in the constructed tree. *Topographer* chooses a root cell in such a manner that the distances between this cell and those cells that are initially set according to, e.g., the prior knowledge, are as short as possible. An initial pseudotime is first assigned to this root node. Every other cell in the dataset is then assigned in order with a pseudotime according to its relative position in the constructed tree. Without loss of generality, the full pseudotime may be set as the interval between 0 and 1 (i.e., $0 \leq \tau \leq 1$).

The Landscape Module Constructs a Quantitative Waddington's Developmental Landscape of Single-Cell Data
Calculation of Cell Potential

After the backbone of a developmental trajectory has been identified and every cell has been endowed with a pseudotime value, the landscape module first estimates the potential of every cell in the dataset and then uses these potentials to construct a quantitative developmental landscape. It is expected that the potential to be introduced can be avoid shortcomings of the pseudo-potential as pointed out in the main text. For this estimation, *Topographer* analogizes transitions between cells at distinct stages of the differentiation process to a random walker who moves randomly between the data points that are randomly scattered in the cell state space. This analogy, which is inspired by Rosvall and Bergstrom's work (Rosvall and Bergstrom, 2008), is reasonable due to both cellular heterogeneity and gene expression noise in the dataset. In addition, it is important that *Topographer* uses the pseudotime information to construct a weighted directed graph **W**.

Specifically, *Topographer* defines the weight of the directed edge from cell α to cell β as

$$W_{\alpha \to \beta} = W_0 e^{-\chi(\tau_\alpha - \tau_\beta)}. \tag{4}$$

(**Supplementary Information** gives a reason for this definition), where τ_α and τ_β represents the pseudotime points for cells α and β respectively, and positive constant χ represents a linearly changing rate that cell α transitions to cell β (this setting implies an assumption, i.e., the evolutional process from one cell to another along the pseudotime is assumed to be linear). The setting of the χ value in general depends on the dataset under consideration (see subsection 3.2.1 in **Supplementary Information** gives a simple discussion) but it may be set as 30 in our cases (i.e., χ=30). It is worth pointing out that the weight defined in such a manner has used the information on the pseudo-temporally ordered cell trajectories, which is a key for the entire calculation.

Then, in order to estimate cell visit probability on a random walk, *Topographer* defines a conditional probability that the random walker moves from cell β to cell α as the relative link weight, given by

$$p_{\beta \to \alpha} = \frac{W_{\beta \to \alpha}}{\sum_\beta W_{\beta \to \alpha}}, \tag{5}$$

which is apparently independent of initial W_0. If the stationary visit probability of cell α is denoted by p_α, then p_α can in principle be derived from a recursive system of the form

$$p_\alpha = \sum_\beta p_\beta p_{\beta \to \alpha}, \tag{6}$$

which represents the probability that the random walker visits the α cell from all the other possible cells. Note that Eq. (6) is actually a master equation (van Kampen, 1992) and can efficiently be solved with the power-iteration method (Booth, 2006). However, to ensure that the unique solution of this equation is independent of the starting node in the directed network, the random walker instead teleports to a random node at a small rate ε with $0 < \varepsilon < 1$ (in simulation, we set $\varepsilon = 0.01$). In addition, to obtain more robust results that depend less on the teleportation parameter ε, it is most often to use teleportation to a node proportional to the total weight of the links to the node (Rosvall and Bergstrom, 2008). Because of these considerations, the resulting stationary visit probability for cell α is modified as

$$p_\alpha = (1-\epsilon)\sum_\beta p_\beta p_{\beta \to \alpha} + \epsilon \frac{\sum_\beta W_{\alpha \to \beta}}{\sum_{\alpha,\beta} W_{\beta \to \alpha}}. \tag{7}$$

Finally, *Topographer* quantifies the potential of every cell in the dataset, according to

$$E_\alpha = -\log p_\alpha, \tag{8}$$

where p_α is given by Eq. (7). Apparently, the potential defined in such a manner has again made use of the information on the identified cell-state transition trajectories due to Eq. (4). We point out that the potential of a cell depends on pseudotime but the pseudo-potential lacks the information on pseudotime.

Scatter Plot of Developmental Landscape

After all the cells in the dataset have been equipped with potentials, all these potentials are then used to construct a Waddington's

landscape for the developmental process. The method is stated as follows. First, dimension reduction is needed for visualization (the tSNE method (van der Maaten and Hinton, 2008) or the PCA method (Hastie et al., 2001) may be used to achieve this purpose). In general, dimension reduction cannot explicitly reflect the information on coordinates in a visualized landscape, e.g., PCA1 and PCA2 in **Figure 3C** do not actually represent components in the dataset. Second, *Topographer* uses the nearest neighbor interpolation method to perform interpolation on a 3-dimensional scattered data set. Specifically, *Topographer* uses ScatteredInterpolant (a function of the MATLAB software) to establish the corresponding relationships between a set of points, (x,y), and a set of cell potentials, E. These relationships, denoted by $E=F(x,y)$, in principle define a curved surface in the 3-dimensional space for the developmental landscape, which in return passes through all the sampling points in the space under consideration. *Topographer* then uses the nearest neighbor interpolation to evaluate this surface at any query point (x_q, y_q), thus obtaining an interpolating value of every known potential given by Eq. (8), i.e., $E_q = F(x_q, y_q)$. Third, a Gaussian kernel is used to smooth interpolation. Finally, the identified developmental trajectory is drawn on the constructed developmental landscape (referring to the thick colored line in **Figure 1A** or the thick green line in **Figure 3C**).

We point out that pseudo-potential cannot correctly reflect the motion of a "ball" in the constructed Waddington's developmental landscape in which the moving ball has lower potential at the beginning than at the end, since a lower cell density implies a higher pseudo-potential according to definitions. **Supplementary Figure 5** shows a difference between potential and pseudo-potential.

The Dynamics Module Estimates Fate Probabilities of Cell Types and Transition Probabilities Between Them From Single-Cell Data

Determining Cell Types

Cell-type dynamics can be characterized by fate and transition probabilities. In order to estimate these probabilities, it is first needed to determine the types of cells in the dataset. For this, *Topographer* adopts the following rules: First, each branch in the identified developmental trajectory is defined as one cell type, and a different branch is defined as a different cell type. Then, each potential well on each branch is defined as one cell subtype, and a different potential well is defined as a different cell subtype. These definitions imply that the number of cell types is equal to that of branches whereas the number of cell subtypes is equal to that of potential wells. It should be pointed out that the cell type determined in such a manner is not unique but depends on the choice of $\tilde{E}$ and δ (their respective definitions above). In the following, we will not distinguish cell type and cell subtype unless confusion arises.

Estimating Transition Probabilities Between Cell Types

Equation (5) has given the conditional probability ($p_{\beta \to \alpha}$) that the random walker moves from cell β to cell α, whereas Eq. (7) has given the stationary visit probability of cell α, i.e., p_α. On the basis of these, *Topographer* estimates the transition probability at which a random walker visits the jth cell type from the ith cell

type (denoted by $q_{i \curvearrowright}$), according to

$$q_{i \curvearrowright j} = \sum_{\alpha \in i, \beta \notin j} q_{\alpha \to \beta}, \qquad (9)$$

and the transition probability at which the random walker exits the ith cell type (denoted by $q_{i \curvearrowright}$), according to

$$q_{i \curvearrowright} = \sum_{\alpha \in i, \beta \notin i} q_{\alpha \to \beta}, \qquad (10)$$

where the unrecorded visit rate on a link, $q_{\beta \to \alpha}$ is given by

$$q_{\beta \to \alpha} = p_\beta p_{\beta \to \alpha}. \qquad (11)$$

Estimating Fate Probabilities of Cell Types

The fate probability for cell type i, denoted by $fate_i$, is defined as

$$fate_i = 1 - q_{i \curvearrowright}, \qquad (12)$$

which implies that a larger transition probability at which the random walker exits cell type i corresponds to a smaller fate probability for this cell type. This definition is in accordance with our intuition, so it is reasonable. Again, we emphasize that the above formulae for transition probability ($q_{i \curvearrowright j}$) and fate probability ($fate_i$) have all made use of the pseudotime information.

The Network Module Infers Marker Gene Networks and Their Pseudo-Temporal Changes

In a complex mixture of cells, correlations of gene expression patterns would arise from differences between different cell lineages. To explore the correlation between the patterns of gene expression across development, *Topographer* constructs a series of GRNs along the pseudotime, which are directed networks for gene-gene interactions. Unsupervised GRNs are then created by GENIE3 (Huynh-Thu et al., 2010) that takes advantage of the random forest machine learning algorithm.

Based on the constructed GRNs, *Topographer* further explores the covariation partners of some particular gene (or genes) using a topological network analysis scheme (Li and Horvath, 2007). The method is to identify the set of those genes that are most closely correlated with a given gene (or genes) of interest and that most closely correlate to each other, at a given pseudotime point (in practical calculations, we use data at a pseudotime window to improve accuracy) (in **Figure 4** of the main text, however, we showed how neighborhood networks of a marker gene change at several representative pseudotime points). **Supplementary Information** provides more details of the method.

The Burst Module Infers Pseudo-Temporal Characteristics of Transcriptional Bursting Kinetics

Transcriptional bursting kinetics can be characterized by BS and BF. As is well known, Gamma distributions can well capture this bursty expression in some cases. *Topographer* uses a Gamma distribution to infer dynamic characteristics of transcriptional bursting kinetics along the cell-state transition trajectories

identified from single-cell RNA-seq data. Assume that this distribution takes the form (Friedman et al., 2006)

$$p(x) = \frac{x^{a-1}}{b^a \Gamma(a)} e^{-\frac{x}{b}}, \qquad (13)$$

where x represents the number of transcripts, a represents the mean BF (i.e., the mean number of mRNA production bursts per cell cycle) whereas b does the mean BS (i.e., the average size of the mRNA bursts), and $\Gamma(\cdot)$ is the common Gamma function.

Thus, in order to infer pseudo-temporal characteristics of transcriptional bursting dynamics, the key is to estimate two parameters a and b from the dataset at every pseudotime point. For this, *Topographer* makes use of the maximum likelihood method (Hastie et al., 2001). Since the number of cells at a single pseudotime point would be very few, *Topographer* uses the cell data in a window of this point to obtain more reliable estimations of a and b.

DATA AVAILABILITY STATEMENT

Single-cell data on development of primary human myoblasts can be downloaded from doi:10.1038/nbt.2859 (Trapnell et al., 2014). A MATLAB package for the *Topographer* algorithm is available through github (https://github.com/cellfate/topographer).

AUTHOR CONTRIBUTIONS

JZ and TZ conceived and designed the work. JZ carried out computer implementation and data analysis. JZ, QN, and TZ interpreted the simulation results. TZ supervised the project, JZ and TZ wrote the original manuscript, and QN contributed to the writing of final manuscript.

FUNDING

ACKNOWLEDGMENTS

SUPPLEMENTARY MATERIAL

The Supplementary Material for this article can be found online at: https://www.frontiersin.org/articles/10.3389/fgene.2019.01280/full#supplementary-material

It provides a complete description of *Topographer* and supplements analysis of artificial and real examples.

REFERENCES

Bendall, S. C., Simonds, E. F., Qiu, P., el-AD, Amir, PO, Krutzik, Finck, R., et al. (2011). Single-cell mass cytometry of differential immune and drug responses across a human hematopoietic continuum. *Science* 332, 687–696. doi: 10.1126/science.1198704

Booth, T. E. (2006). Power iteration method for the several largest eigenvalues and eigenfunctions. *Nucl. Sci. Eng. J. Am. Nucl. Soc.* 154, 48–62. doi: 10.13182/NSE05-05

Cam, L. L. (1991). Maximum likelihood-an introduction. *Int. Statist. Rev.* 58, 153–171. doi: 10.2307/1403464

Chan, T. E., Stumpf, M. P. H., and Babtie, A. C. (2017). Gene regulatory network inference from single-cell data using multivariate information measures. *Cell Syst.* 5, 251–267. doi: 10.1016/j.cels.2017.08.014

Chen, L., Liu, R., Liu, Z. P., Li, M., and Aihara, K. (2012). Detecting early-warning signals for sudden deterioration of complex diseases by dynamical network biomarkers. *Sci. Rep.* 2, 18–20. doi: 10.1038/srep00342

Friedman, N., Cai, L., and Xie, X. S. (2006). Linking stochastic dynamics to population distribution: An analytical framework of gene expression. *Phys. Rev. Lett.* 97, 168302. doi: 10.1103/PhysRevLett.97.168302

Furusawa, C., and Kaneko, K. (2012). A dynamical-systems view of stem cell biology. *Science* 338, 215–217. doi: 10.1126/science.1224311

Gupta, P. B., Fillmore, C. M., Jiang, G., Shapira, S. D., Tao, K., Kuperwasser, C., et al. (2011). Stochastic state transitions give rise to phenotypic equilibrium in populations of cancer cells. *Cell* 146, 633–644. doi: 10.1016/j.cell.2011.07.026

Gut, G., Tadmor, M. D., Pe'er, D., Pelkmans, L., and Liberali, P. (2015). Trajectories of cell-cycle progression from fixed cell populations. *Nat. Methods* 12, 951–954. doi: 10.1038/nmeth.3545

Haghverdi, L., Büttner, M., Wolf, F. A., Buettner, F., and Theis, F. J. (2016). Diffusion pseudotime robustly reconstructs lineage branching. *Nat. Methods* 13, 845–848. doi: 10.1038/nmeth.3971

Hastie, T., Tibshirani, R., and Friedman, J. (2001). *The Elements of Statistical Learning* (New York: Springer). doi: 10.1007/978-0-387-21606-5

Huynh-Thu, V. A., Irrthum, A., Wehenkel, L., and Geurts, P. (2010). Inferring regulatory networks from expression data using tree-based methods. *PloS One* 5, e12776. doi: 10.1371/journal.pone.0012776

Kafri, R., Levy, J., Ginzberg, M. B., Oh, S., Lahav, G., and Kirschner, M. W. (2013). Dynamics extracted from fixed cells reveal feedback linking cell growth to cell cycle. *Nature* 494, 480–483. doi: 10.1038/nature11897

Kim, J. K., and Marioni, J. C. (2013). Inferring the kinetics of stochastic gene expression from single-cell RNA-sequencing data. *Genome Biol.* 14, R7. doi: 10.1186/gb-2013-14-1-r7

Klein, A. M., Mazutis, L., Akartuna, I., Tallapragada, N., Veres, A., Li, V., et al. (2015). Droplet barcoding for single-cell transciptomics applied to embryonic stem cell. *Cell* 161, 1187–1101. doi: 10.1016/j.cell.2015.04.044

Larson, D. R. (2011). What do expression dynamics tell us about the mechanism of transcription? *Curr. Opin. Genet. Dev.* 21, 591–599. doi: 10.1016/j.gde.2011.07.010

Larsson, A. J. M., Johnsson, P., Hagemann-Jensen, M., Hartmanis, L., Faridani, O. R., et al. (2019). Genomic encoding of transcriptional burst kinetics. *Nature* 565 (7738), 251–254. doi: 10.1038/s41586-018-0836-1

Li, H., and Horvath, S. (2007). Network neighborhood analysis with the multimode topological overlap measure. *Bioinformatics* 23, 222–231. doi: 10.1093/bioinformatics/btl581

Li, C., and Wang, J. (2013). Quantifying cell fate decisions for differentiation and reprogramming of a human stem cell network: landscape and biological paths. *PloS Comput. Biol.* 9, e1003165. doi: 10.1371/journal.pcbi.1003165

Li, C., and Wang, J. (2013). Quantifying Waddington landscapes and paths of non-adiabatic cell fate decisions for differentiation, reprogramming and transdifferentiation. *J. R. Soc. Interface.* 10, 20130787. doi: 10.1098/rsif.2013.0787

Li, C., and Wang, J. (2014). Landscape and flux reveal a new global view and physical quantification of mammalian cell cycle. *Proc. Natl. Acad. Sci. U.S.A.* 111 (39), 14130–14135. doi: 10.1073/pnas.1408628111

Li, C., and Wang, J. (2015). Quantifying the landscape for development and cancer from a core cancer stem cell circuit. *Cancer Res.* 75, 2607–2618. doi: 10.1158/0008-5472.CAN-15-0079

Lummertz da Rocha, E., Rowe, R. G., Lundin, V., Malleshaiah, M., Jha, D. K., Rambo, C. R., et al. (2018). Reconstruction of complex single-cell trajectories using CellRouter. *Nat. Commun.* 9, 892. doi: 10.1038/s41467-018-03214-y

Moignard, V., and Göttgens, B. (2016). Dissecting stem cell differentiation using single cell expression profiling. *Curr. Opin. Cell Biol.* 43, 78–86. doi: 10.1016/j.ceb.2016.08.005

Mojtahedi, M., Skupin, A., Zhou, J., Castaño, I. G., Leong-Quong, R. Y. Y., Chang, H., et al. (2016). Cell fate decision as high-dimensional critical state transition. *PloS Biol.* 14 (12), e2000640. doi: 10.1371/journal.pbio.2000640

Moris, N., Pina, C., and Arias, A. M. (2016). Transition states and cell fate decisions in epigenetic landscapes. *Nat. Rev. Genet.* 17, 693–603. doi: 10.1038/nrg.2016.98

Olsson, A., Venkatasubramanian, M., Chaudhri, V. K., Aronow, B. J., Salomonis, N., Singh, H., et al. (2016). Single-cell analysis of mixed-lineage states leading to a binary cell fate choice. *Nature* 537, 698–702. doi: 10.1038/nature19348

Perié, L., Duffy, K. R., Kok, L., and de Boer, R. J. (2015). Schumacher TN. the branching point in erythro-myeloid differentiation. *Cell* 163, 1655–1662. doi: 10.1016/j.cell.2015.11.059

Rodriguez, A., and Laio, A. (2014). Clustering by fast search and find of density peaks. *Science* 344, 1492–1496. doi: 10.1126/science.1242072

Rosvall, M., and Bergstrom, C. T. (2008). Maps of random walks on complex networks reveal community structure. *Proc. Natl. Acad. Sci. U.S.A.* 105, 1118–1123. doi: 10.1073/pnas.0706851105

Saelens, W., Cannoodt, R., Todorov, H., and Saeys, Y. (2019). A comparison of single-cell trajectory inference methods: towards more accurate and robust tools. *Nat. Biotechnol.* 37 (5), 547–554. doi: 10.1038/s41587-019-0071-9

Setty, M., Tadmor, M. D., Reich-Zeliger, S., Angel, O., Salame, T. M., Kathail, P., et al. (2016). Wishbone identifies bifurcating developmental trajectories from single-cell data. *Nat. Biotechnol.* 34, 637–645. doi: 10.1038/nbt.3569

Shin, J., Berg, D. A., Zhu, Y., Shin, J. Y., Song, J., Bonaguidi, M. A., et al. (2015). Single-cell RNA-Seq with waterfall reveals molecular cascades underlying adult neurogenesis. *Cell Stem Cell* 17, 360–372. doi: 10.1016/j.stem.2015.07.013

Svensson, V., Natarajan, K. N., Ly, L. H., Miragaia, R. J., Labalette, C., Macaulay, I. C., et al. (2017). Power analysis of single-cell RNA-sequencing experiments. *Nat. Methods* 14, 381–387. doi: 10.1038/nmeth.4220

Tanay, A., and Regev, A. (2017). Scaling single-cell genomics from phenomenology to mechanism. *Nature* 541, 331–338. doi: 10.1038/nature21350

Trapnell, C., Cacchiarelli, D., Grimsby, J., Pokharel, P., Li, S., Morse, M., et al. (2014). The dynamics and regulators of cell fate decisions are revealed by pseudotemporal ordering of single cells. *Nat. Biotechnol.* 32, 381–386. doi: 10.1038/nbt.2859

Trapnell, C. (2015). Defining cell types and states with single-cell genomics. *Genome Res.* 25, 1491–1498. doi: 10.1101/gr.190595.115

van der Maaten, L. J. P., and Hinton, G. E. (2008). Visualizing high-dimensional data with t-SNE. *J. Machin. Learn. Res.* 9, 2579–2505.

van Kampen, N. G. (1992). *Stochastic Process in Physics and Chemistry* (Amsterdam: North-Holland).

Waddington, C. H. (1957). *The strategy of the genes: a discussion of some aspects of theoretical biology* (London: Allen and Unwin).

Wang, J., Zhang, K., Xu, L., and Wang, E. (2011). Quantifying the Waddington landscape and biological paths for development and differentiation. *Proc. Natl. Acad. Sci. U.S.A.* 108, 8257–8262. doi: 10.1073/pnas.1017017108

Wu, J. C., and Tzanakakis, E. S. (2012). Contribution of stochastic partitioning at human embryonic stem cell division to NANOG heterogeneity. *PloS One* 7, e50715. doi: 10.1371/journal.pone.0050715

Zhang, J. J., Nie, Q., and Zhou, T. S. (2018). Topographer reveals dynamic mechanisms of cell fate decisions from single-cell transcriptomic data. *bioRxiv* 215205. doi: 10.1101/251207

Ziegenhain, C., Vieth, B., Parekh, S., Reinius, B., Guillaumet-Adkins, A., Smets, M., et al. (2017). Comparative analysis of single-cell RNA sequencing methods. *Mol. Cell* 65, 631–643. doi: 10.1016/j.molcel.2017.01.023